HHS Public Access

Author manuscript

*FASEB J.* Author manuscript; available in PMC 2023 May 01.

Published in final edited form as:

*FASEB J.* 2022 May ; 36(5): e22331. doi:10.1096/fj.202200010RR.

# Hypoxia-induced blood-brain barrier dysfunction is prevented by pericyte-conditioned media via attenuated actomyosin contractility and claudin-5 stabilization

**John J. Jamieson**[1,2], **YingYu Lin**[1,2], **Nicholas Malloy**[3], **Daniel Soto**[3], **Peter C. Searson**[2,4,5,*], **Sharon Gerecht**[1,2,4,5,6,*]

[1]Department of Chemical and Biomolecular Engineering, Johns Hopkins University, 3400 North Charles Street, Baltimore, MD, 21218, USA

[2]Institute for Nanobiotechnology, 100 Croft Hall, Johns Hopkins University, 3400 North Charles Street, Baltimore, MD, 21218, USA

[3]Solomon H. Snyder Department of Neuroscience, Johns Hopkins University School of Medicine, Baltimore, MD, 21205, USA

[4]Department of Biomedical Engineering, Johns Hopkins University, 720 Rutland Avenue, Baltimore, MD, 21205, USA

[5]Department of Materials Science and Engineering, Johns Hopkins University, 3400 North Charles Street, Baltimore, MD, 21218, USA

[6]Department of Biomedical Engineering, Duke University, Duke, NC 27708, USA

## Abstract

The blood-brain barrier (BBB) regulates molecular and cellular entry from the cerebrovasculature into the surrounding brain parenchyma. Many diseases of the brain are associated with dysfunction of the BBB, where hypoxia is a common stressor. However, the contribution of hypoxia to BBB dysfunction is challenging to study due to the complexity of the brain microenvironment. In this study, we used a BBB model with brain microvascular endothelial cells and pericytes differentiated from iPSCs to investigate the effect of hypoxia on barrier function. We found that hypoxia-induced barrier dysfunction is dependent upon increased actomyosin contractility and is associated with increased fibronectin fibrillogenesis. We propose a role for actomyosin contractility in mediating hypoxia-induced barrier dysfunction through modulation of junctional claudin-5. Our findings suggest pericytes may protect brain microvascular endothelial cells from hypoxic stresses and that pericyte-derived factors could be candidates for treatment of pathological barrier-forming tissues.

[*]Corresponding authors: sharon.gerecht@duke.edu and searson@jhu.edu.

Author contributions

Conceptualization, PS and SG; experimentation, JJ, YL, NM, DS; data analysis, JJ, YL, NM, DS, PS, and SG; writing, reviewing, & editing, JJ, PS, and SG; supervision, PS and SG; funding acquisition, PS and SG.

Data Availability Statement

The data that support the findings of this study are available in the methods and/or supplementary material of this article.

Conflict of Interest Statement

The authors declare that they have no competing interests

**Keywords**

Blood-brain barrier; hypoxia; brain microvascular endothelial cells; pericytes; induced pluripotent stem cells; tissue engineering; contractility; transendothelial electrical resistance

## Introduction

The blood-brain barrier (BBB) regulates molecular and cellular entry from the brain microvasculature into the surrounding brain parenchyma (1–3). The cellular components of the BBB include brain microvascular endothelial cells (BMECs) supported by pericytes and astrocytes. BMECs are highly specialized, with a range of transporters and efflux pumps to regulate the transport of nutrients and other essential molecules, and tight junction (TJs), which restrict paracellular transport. Dysfunction of the BBB can lead to extravasation of serum proteins and contribute to inflammatory responses, plaque formation, and neurotoxicity (4).

Hypoxia is a common stressor associated with BBB dysfunction in diseases and medical conditions, including ischemic stroke, traumatic brain injury, neurodegenerative diseases, and altitude sickness (5, 6). For example, affected brain regions receive limited blood flow during ischemic stroke and can become hypoxic within minutes (5). A complex cascade of events occurs following the initial event, including excitotoxicity-induced neuronal death, inflammation, edema, and disruption of the BBB. These effects continue to manifest even after blood flow has been restored. The timeline of ischemia-induced BBB disruption remains controversial. In animal ischemia models, disruption occurs in two phases, at 4 – 6 hours and 2 – 3 days post-ischemia (7). However, a clinical study reported continuous disruption peaking at 6 – 48 hours post-ischemia (8). The contribution of hypoxia to BBB dysfunction in ischemia is difficult to study since many factors change simultaneously, and independent control of these variables is limited *in vivo*.

*In vitro* BBB models provide a means to examine specific cause-and-effect relationships in a reductive manner. Studies of BMECs subjected to hypoxic conditions have demonstrated phosphorylation or delocalization of TJ proteins, including claudin-5 and occludin (9). These changes appear to be downstream of hypoxia induced transcription factors (HIFs) and may be mediated in part through increased secretion of VEGF (10, 11). Tight junction proteins are connected to the cytoskeleton via various linkers, most notably zonula occludens-1 (ZO-1). Thus, cytoskeletal changes can influence TJs, and in turn, barrier function (12). Hypoxia has been shown to affect cytoskeletal organization through HIFs, although changes appear to vary across cell types and experimental conditions (13). However, several studies have shown that hypoxia increases actin stress fiber assembly and actomyosin contractility in non-brain specific endothelial cells (12–16). This can occur either via Rho GTPase RhoA and its downstream activators ROCK-1 and −2, or due to increases in MLCK activity. Contractility is also directly linked to extracellular matrix (ECM) assembly, and profound changes to ECM organization and structure have been observed in response to hypoxia in multiple cell types, including ECs. These include

increased production and remodeling of ECM proteins, including fibronectin, collagens, and laminins (17).

Studies of the role of supporting cell types on barrier function in hypoxia have been inconsistent. While some studies have shown that co-cultured pericytes and/or glial cells provide protective cues (18, 19), others found enhanced hypoxic injury, for example, by secreting angiogenic factors such as VEGF (11, 20, 21). However, most of these studies have been performed with ECs that do not possess physiological barrier function.

Various differentiation strategies have been developed to generate brain microvascular endothelial cell-like cells (iBMECs) from induced pluripotent stem cells. Confluent monolayers of iBMECs display expression of important endothelial- and BBB-specific markers at the protein and gene level (22, 23). We have also previously differentiated pericyte-like cells (iPCs) from iPSCs and found that their conditioned medium can rescue barrier function in stressed iBMEC monolayers (24). Here we investigate the effect of hypoxia on barrier function of iBMEC monolayers and show that hypoxia-induced barrier dysfunction is dependent upon increased actomyosin contractility. We propose a role for actomyosin contractility in mediating hypoxia-induced barrier dysfunction through modulation of junctional claudin-5. Our findings suggest pericytes may protect BMECs from hypoxic stresses and that pericyte-derived factors could provide therapeutic benefits to barrier-forming tissues.

## Material and Methods

### iBMEC differentiation

WTC-ZO1-GFP and WTC-ACTB-GFP hiPSC (Allen Cell Institute) and BC1 hiPSC (kind gift from Dr. Linzhao Cheng) lines were maintained and differentiated to iBMECs as previously described (24) with minor modifications described in Supplemental Experimental Procedures.

### iPC differentiation and PCM collection

BC1 hiPSCs were differentiated to iPCs as previously described (24). Pericyte-conditioned medium (PCM) was produced by culturing iPCs in iBMEC medium for 48 h. PCM was then collected and frozen in aliquots at −20 ˚C until use. Fresh iBMEC medium prepared from the same batch of serum was also frozen until use.

### Transendothelial electrical resistance (TEER)

TEER was measured on 24-well Transwell inserts with a 0.4 μm pore size (Corning 3470), as previously described (24). An EVOM2 system (World Precision Instruments) with a STX2 probe was used to measure the resistance (Ω). TEER values were reported as Ω $cm^2$ following subtraction of the resistance of an acellular Transwell insert and correction for the membrane area (0.33 $cm^2$). All TEER experiments were performed with at least 2 independent differentiations. We used TEER rather than solute permeability as a proxy for barrier function since the time dependence is much easier to measure and permeability coefficients have limited value in cases where defects in the monolayer lead to focal leaks.

### Hypoxic treatment

Two days after seeding, iBMECs were placed in a modular hypoxia chamber (Billups-Rothenberg) filled with a gas mixture containing 1% $O_2$, 5% $CO_2$, and 94% $N_2$ and stored in a standard cell culture incubator alongside cells cultured in atmospheric oxygen. After 48 h, iBMECs were removed from the modular chamber and immediately subjected to TEER measurements and/or other assays as indicated.

### Immunocytochemistry and image analysis

The fixation methods and antibodies used are tabulated in the Supplemental Experimental Procedures. Cells were imaged on a LSM 800 microscope using ZEN Blue software (Zeiss). Tight junctions and fibronectin fibrils were each quantified using FIJI/Image J (NIH), with detailed procedures for each found in the Supplemental Experimental Procedures.

### Mass Spectrometry Proteomics

SDS-PAGE was performed on fresh standard iBMEC media and PCM using pre-cast 4–12% Bis-Tris gradient gels with MES running buffer. Coomassie Blue R-250 was used to visualize the total protein content of each media. The region with the most prominent banding difference was excised from the gel for each condition. Samples were digested with trypsin and analyzed via LC-MS. Scaffold 4 (Proteome Software) was used to analyze the results, filtered by the following settings: 95% protein threshold, minimum of 2 peptides detected, and 95% peptide threshold.

### Statistical analysis

GraphPad Prism 9 was used for statistical analysis. The student's t-test was employed to compare two conditions, while ANOVA with multiple comparisons was used for tests with three or more conditions. P-values were multiplicity adjusted using either the Dunnett or Tukey multiple comparisons tests, as appropriate. Differences were considered statistically significant for $P < 0.05$, with the following thresholds: * $p < 0.05$, ** $p < 0.01$, *** $p < 0.001$, and **** $p < 0.001$. The number of replicates for each experiment is described in the corresponding figure caption.

## Results

### Hypoxia decreases barrier function by disrupting junctional claudin-5

To study the effects of hypoxia on BBB function, human brain microvascular endothelial-like cells (iBMECs), differentiated from human iPSCs, were exposed to 1% $O_2$. iBMECs cultured on Transwell inserts typically attained maximum transendothelial electrical resistance (TEER) within 1 – 2 days, and hence hypoxic conditions were initiated 2 days after seeding (Fig. 1A). After 24 hours in 1% $O_2$, we observed no change in TEER (Fig. 1B). Interestingly, when the treatment time was extended to 48 hours, TEER sharply declined by 60% relative to a control maintained in an incubator at ~20% $O_2$.

Since TJs restrict paracellular permeability, we next examined gene and protein expression of the two main TJ proteins in the BBB, claudin-5 and occludin, in response to 48 h hypoxia. Quantitative PCR analysis demonstrated that claudin-5 transcripts (*CLDN5*)

decreased by 37% in hypoxia, while occludin transcripts (*OCLN*) did not change (Fig. 1C). However, total protein levels measured via western blot were unchanged for both proteins (Fig. 1D–F). Next, we examined the localization of claudin-5 and occludin in response to hypoxia. Claudin-5 localization was noticeably disrupted by hypoxia, as evidenced by the frayed cell-cell junctions (Fig. 1G). Quantitatively, we measured a 35% decrease in junctional claudin-5, and a 10% decrease in the ratio of junctional to total claudin-5, suggesting internalization (Fig. 1H). In contrast to claudin-5, we did not observe changes in the appearance or localization of occludin. Nor did we observe changes in the appearance or localization of the TJ-associated protein ZO-1 (Fig. S1). Taken together, these results indicate that a 48 h treatment with 1% $O_2$ disrupts barrier function by disruption of junctional claudin-5.

## Hypoxia modulates claudin-5 via increased actomyosin contractility

Previous studies in endothelial and epithelial cells have highlighted a complex relationship between actomyosin contractility and barrier function (25). Optimal levels of contractility promote the formation and maintenance of a stable barrier, however, in various pathological settings, including hypoxia and inflammation, an increase in contractility, particularly in actin stress fibers, can compromise barrier function (12). We hypothesized that hypoxia could lead to TJ disassembly by increasing cell contractility beyond normal levels (Fig. 2A). To test this hypothesis, we exposed iBMECs to 1% $O_2$ for 48 hours and then examined cytoskeletal organization (Fig. 2B). We observed a remarkable increase in the presence of ventral stress fibers, as well as an increase in phosphorylated myosin light chain 2 (pMLC2) overlapping these fibers, suggesting elevated contractile activity in response to hypoxia (Fig. 2C).

We then confirmed that suppression of contractility prevented loss of TJs during hypoxia. First, we showed that adding the ROCK1/ROCK2 inhibitor Y-27632 (10μM) during hypoxia prevented the formation of actin stress fibers and reduced pMLC (Fig. 2C). We then examined claudin-5 localization and found that Y-27632 enriched claudin-5 at junctions in hypoxia (Fig.2D–F). Consistent with the protection of TJs, we discovered that Y-27632 addition blocked 67% of the decrease in TEER caused by hypoxia (Fig. 2G).

To confirm that elevated actomyosin contractility was responsible for hypoxia-induced barrier dysfunction, we utilized an alternative pharmacological approach to reduce contractility. Blebbistatin (10μM), an ATPase inhibitor of non-muscle myosin II, greatly reduced actin stress fiber formation in hypoxia, resembling the effects of Y-27632 (Fig. S2). Likewise, blebbistatin similarly protected TEER and claudin-5 during hypoxia (Fig. 2D–G). Finally, we examined whether further increasing contractility would exacerbate barrier dysfunction in hypoxia by exposing cells to the phosphatase inhibitor calyculin A (2nM), which inhibits the dephosphorylation of myosin II, increasing its activity and increasing cell contractility (Fig. S3A). We found that calyculin A treatment further disrupted junctional claudin-5 localization and sharply decreased TEER (Fig. 2D–G). Calyculin A also appeared to cause the formation of small gaps between some adjacent cells as indicated by ZO-1 staining (Fig. S3B). Overall, these results show that iBMECs exhibit increased actomyosin

contractility in response to hypoxia and that claudin-5 can either be protected by inhibiting actomyosin activity or damaged by activation of actomyosin activity.

## Pericyte-conditioned medium protects barrier function during hypoxia via normalized cell contractility and claudin-5 stabilization

In a prior study we found that co-culture with pericytes or the presence of pericyte-conditioned medium (PCM) could restore barrier function in stressed iBMECs (24). These results prompted us to hypothesize that PCM may protect barrier function during hypoxia. In the previous study we found that iBMEC monolayers with induced pericytes (iPCs) seeded on top did not remain confluent (24). Thus, in the current study we focused on using iPC-conditioned medium that showed a similar effect. Induced pericytes differentiated from iPSCs along a mesodermal lineage as previously reported (24, 26), were cultured in iBMEC medium for 2 days to generate PCM (Fig. 3A, S4). iBMECs were then exposed to hypoxia in the presence of either PCM or standard iBMEC media (Fig. 3B). iBMECs exhibited significantly higher TEER when exposed to hypoxia in PCM compared with standard iBMEC medium (1276±173 vs. 422±134 Ω $cm^2$; mean±SD) (Fig. 3C). Additionally, PCM prevented hypoxia-induced decreases in *CLDN5* expression and junctional claudin-5 as measured by immunofluorescence (Fig. 3D–F). As iPCs were exposed to atmospheric $O_2$ during PCM production, we also investigated whether the effect on barrier function would change if iPC were instead maintained under hypoxic conditions producing hypoxic-PCM (HPCM). We found that both HPCM and PCM exhibited a similar TEER-protective effect when applied to iBMEC during hypoxia (Fig. S5), thus PCM was used for all subsequent studies. To check whether our findings could be secondary to differences in cell density across conditions, we measured monolayer cell density and found that hypoxia generally reduced monolayer density by 20–30%, but that this was not affected by the addition of PCM or Y-27632 (Fig. S6). We next determined whether the barrier protection conferred by PCM during hypoxia was mediated by changes to the cytoskeletal structure and actomyosin contractility. In contrast to results in standard medium, in PCM we observed fewer stress fibers and reduced pMLC (Fig. 3G). To confirm this finding, total pMLC levels were assessed via western blot (Fig. 3H). We found that hypoxia increased pMLC levels by 40% in standard media but that this increase was entirely prevented by PCM (Fig. 3I). Together these results demonstrate that PCM protects barrier function of iBMEC monolayers during hypoxia by normalizing contractility and preventing the loss of claudin-5 at cell-cell junctions.

## Hypoxia and PCM alter basement membrane organization in iBMEC monolayers

To identify potential regulators of contractility, claudin-5, and barrier function that may differ between standard medium and PCM, we performed SDS-PAGE on fresh iBMEC medium and PCM. Differences were observed in species with molecular weight > 200 kDa, as visualized by a Coomassie Blue R-250 total protein stain. The gel region with the most prominent banding difference between the two conditions was excised and analyzed via mass spectrometry (Fig. 4A). Eighty-five different proteins were identified in these samples, of which 45 were increased in PCM, 26 were decreased, and 14 were unchanged (see Table S1). The most abundant protein was fibronectin, which was increased by 35% in PCM relative to standard medium (270 vs. 198 exclusive unique spectrum count)

(Fig. 4B). In addition, we noted increases in a variety of ECM or ECM-related proteins, particularly collagens and laminins. The increased content of ECM proteins in PCM led us to hypothesize that iBMEC monolayers cultured in PCM may exhibit changes in basement membrane (BM) organization.

To explore this, we exposed iBMEC monolayers to hypoxia or atmospheric $O_2$ in standard media, or to hypoxia in PCM (Fig. 4C) and then examined collagen IV and fibronectin localization (Fig. 4D). In atmospheric $O_2$, we observed sporadic deposits of collagen IV and fibronectin in limited networks along a fraction of the cell-cell junctions. In hypoxia, these networks were notably more extensive, contacting nearly every cell in the monolayer. However, in hypoxia with PCM, both collagen IV and fibronectin networks were less prevalent. This suggests that the more extended networks induced by hypoxia were associated with a leakier barrier and that either the production or degradation of BM proteins may be modified by PCM.

We next assessed whether these differences in BM organization resulted from changes in iBMEC gene expression during hypoxia, as we have previously observed in endothelial progenitor cells (17). Collagen IV (*COL4A1*), laminin (*LAMC1*), and fibronectin (*FN1*) expression each increased in hypoxia, although these differences were not significant (Fig. 4E). PCM did not affect *COL4A1* or *LAMC1* expression, however, PCM decreased *FN1* expression, suggesting iBMECs may produce less endogenous fibronectin when cultured in PCM, negating hypoxia-driven increases in *FN1*. In summary, PCM was enriched in a variety of soluble ECM proteins, and iBMECs cultured in PCM exhibited changes in the production and deposition of BM proteins that opposed the effects of hypoxia.

Interestingly, despite the observed differences in fibronectin and collagen IV deposition, exogenous addition of these proteins into standard medium before 48 h hypoxia treatment did not prevent TEER reduction (Fig. 4F). Nor did the addition of Matrigel, which contains a diverse mixture of ECM proteins, most notably laminin. However, the accumulation of ECM is a balance between synthesis and degradation. Therefore, we examined the proteases and protease inhibitors in iBMEC monolayers exposed to hypoxia or atmospheric $O_2$ in standard medium, or to hypoxia in PCM. We identified 2 proteases (ADAMTS1 and uPA/Urokinase) and 3 protease inhibitors (TFPI, TFPI-2, and TIMP-2) that were highly elevated in iBMECs cultured in PCM (Fig. 4G). We then added recombinant forms of these proteins to the standard medium during hypoxia, but this did not affect TEER. These findings suggest that: (1) PCM contains a richer mixture of both proteases and protease inhibitors than standard media, and (2) the proteases/protease inhibitors that we detected most elevated in PCM could not reproduce the barrier-protective effects of PCM. The diversity of these enzymes and their unique functionalities make them difficult to study in this context but could be an area for further investigation. Overall, the results from the protease/protease inhibitor profile and our examination of BM protein localization suggest that changes in collagen IV and fibronectin deposition in response to hypoxia compared to PCM play an important role in barrier function of iBMEC monolayers.

## Fibronectin fibrillogenesis is dependent upon cellular contractility and is accelerated in hypoxia but attenuated by PCM or TGF-β inhibition

We next sought to understand how differences in cellular contractility may relate to differences in basement membrane organization. We chose to focus on fibronectin due to its role in the early stages of basement membrane formation: the provisional fibronectin scaffold guides the assembly of many other ECM proteins, including collagens and fibrillins (27–29). Previous reports have demonstrated bidirectional relationships between contractility and fibronectin fibrillogenesis, where cells require contractility to physically remodel surrounding ECM (30–32). However, cells also receive cytoskeletal organization mechanical cues their microenvironment (33, 34). Here we assessed fibrillogenesis across our oxygen and media conditions and in response to varying levels of contractility, as modulated through the addition of Y-27632 or calyculin A. For this experiment, we used iBMECs expressing GFP-tagged beta-actin and confirmed the expected differences in stress fiber formation across our conditions, as well as verified expected claudin-5 differences through immunostaining (Fig. S7).

In atmospheric $O_2$, we observed both fibrillar and adsorbed fibronectin (FN) patterns (Fig. 5A–D), whereas in hypoxia, we observed a more extensive fibrillar meshwork with increased fibril area. The addition of Y-276332 during hypoxia resulted in a significant reduction in fibril area and increased adsorbed FN (note the appearance of adsorbed FN in the acellular condition in Fig. 5A). Likewise, in hypoxia with PCM, we observed predominantly adsorbed FN with short nascent fibrils scattered throughout, suggesting limited fibrillogenesis. However, when we enhanced contractility in PCM using calyculin A (2nM), we observed extensive fibril assembly and minimal remaining adsorbed FN. Overall, these results suggest that cellular contractility drives fibronectin fibrillogenesis in iBMEC monolayers and explains how the variation in contractility levels across our conditions leads to differences in BM organization (Fig. 5B).

As a result of its established roles inducing cellular contractility and FN fibrillogenesis, we next considered whether TGF-β signaling might play a role in hypoxia-induced barrier dysfunction. The addition of the TGF-β inhibitor SB431542 (20 μM) during hypoxia reduced FN fibrillogenesis, as measured by fibril area, without significantly altering adsorbed FN (Fig. 5E–F, S8). We also observed protection of claudin-5 by SB431542 during hypoxia, as demonstrated by improved junctional continuity (Fig. 5E, 5G). Junctional claudin-5 intensity with SB431542 was similar to PCM, although still somewhat reduced relative to atmospheric $O_2$ controls. Lastly, we found that the inclusion of SB431542 protected against hypoxia-induced TEER decline (Fig. 5H). Interestingly, however, TEER values were still lower than PCM. Thus, TGF-β signaling appears to contribute to TEER decline during hypoxia, however, inhibition of this pathway does not protect barrier function as effectively as PCM. Overall, our data demonstrate that FN assembly in iBMEC monolayers is: (1) driven in part by TGF-β signaling, (2) dependent upon actomyosin contractility, and (3) associated with reduced junctional claudin-5 and barrier function.

## Discussion

Hypoxia is an important stressor in multiple pathologies where BBB dysfunction is observed. However, it can be challenging to isolate the downstream effects of hypoxia from those mediated by other factors, including inflammation, edema, and ROS, as well as the contributions of surrounding cell types. In this study, we utilized an *in vitro* approach to examine the specific effects of hypoxia on barrier function in iBMEC monolayers and the mechanisms through which these effects occur. Although several studies have investigated this previously (9, 11, 19, 35, 36), most have been performed on primary or immortalized cells with baseline barrier function much lower than estimated *in vivo* values (1,500 – 6,000 Ω $cm^2$) (3). For our study, we used iBMECs with TEER values of ~2,000 Ω $cm^2$, which have been shown to respond to hypoxia partially through modulation of the HIF pathway (10).

We found that iBMEC monolayers exhibited a 50–60% decrease in TEER after exposure to 1% $O_2$ for 48 h. This decrease was associated with disruption to junctional claudin-5, while occludin remained relatively unchanged and intact at cell-cell junctions, in agreement with a previous study using similarly differentiated cells (10).

The roles of pericytes and astrocytes in hypoxia/ischemia are complex and poorly understood. The inclusion of pericytes or astrocytes in BBB models has inconsistent effects on barrier function even in atmospheric $O_2$ (37), and varied effects are also observed in hypoxia. Pericytes and astrocytes respond to hypoxia by secreting various growth factors and cytokines that can either promote (e.g. ANG-1) or diminish (e.g. VEGF, TGF-β) EC barrier function (11). Two-photon microscopy in mouse models has revealed that pericytes secrete MMP-9 in response to ischemia, leading to localized leaks in the cerebrovasculature (38). Pericytes in the brain arise from different lineages depending on region, with forebrain pericytes arising from neural crest instead of mesoderm, which produces mural cells in most other body tissues. For this study we used mesodermal-derived iPCs, although other recent studies have demonstrated that neural crest-derived iPCs have a similar ability to promote barrier function (39, 40).

In previous work, we showed that the co-culture of iPSC-derived pericytes or pericyte conditioned medium rescued the barrier function of stressed iBMECs (24). Here we showed that PCM prevented claudin-5 disruption and maintained relatively high TEER during hypoxia. We also found that PCM largely prevented the dramatic cytoskeletal reorganization in iBMEC monolayers in response to hypoxia, which included the formation of thick ventral stress fibers and regions of intense pMLC, suggestive of high cellular contractility. Many studies have observed increased contractility in response to inflammatory cues or hypoxia, usually mediated by increased RhoA signaling or MLCK activity (15, 41). Activation of these pathways has been shown to lead to inter-endothelial gap formation and the phosphorylation and internalization of TJ proteins (12, 42, 43).

We also observed striking differences in basement membrane organization in iBMEC monolayers in hypoxia or PCM. Fibronectin and collagen IV networks were much more extensive in hypoxia compared to culture in PCM. This finding is in agreement with studies reporting increased production of extracellular matrix in response to hypoxia (17,

44, 45). Closer examination revealed marked differences in the extent of fibrillogenesis that correlated with differences in cellular contractility, consistent with the established role of mechanical stretching of fibronectin dimers exposing self-association sites to promote polymerization into insoluble fibrils (30, 31). However, assembled fibronectin has also been shown to increase cell contractility and affect cell behaviors such as increased migration, spreading, and angiogenesis (29, 33, 34, 46). When fibrillogenesis was blocked, stress fiber formation and endothelial hyperpermeability were prevented (47).

The pleiotropic cytokine TGF-β has been shown to coordinate with hypoxia during fibrillogenesis (17, 45, 48, 49). Thus, we examined the role of TGF-β signaling in iBMEC monolayers during hypoxia. Inhibition of TGF-β using SB431542 led to reduced fibrillogenesis and improved claudin-5 localization and TEER. Thus, TGF-β signaling in iBMECs during hypoxia increases fibrillogenesis and decreases barrier function. These results are consistent with a recent study demonstrating improved TEER and TJ protein localization resulting from TGF-β inhibition (50).

In summary, we report the effects of hypoxia on the barrier function of iBMEC monolayers. We show that hypoxia disrupts junctional claudin-5 in a manner that is dependent upon TGF-β signaling and RhoA-mediated actomyosin contractility. We also show that hypoxia stimulates fibronectin fibrillogenesis in a process that may further elevate contractility and disrupt cell-cell junctions. However, this hypoxia-induced barrier dysfunction is prevented by the presence of PCM, which reduces both contractility and fibrillogenesis, leading to improved claudin-5 localization and barrier function. These results support the hypothesis that pericytes or pericyte-derived factors may be candidates for treatment of diseases involving elevated cellular contractility, fibrosis, or barrier dysfunction.

## Supplementary Material

Refer to Web version on PubMed Central for supplementary material.

## Acknowledgements

We thank the members of the Searson and Gerecht laboratories for insightful discussions throughout the course of these studies. JJ acknowledges fellowships from the American Heart Association (19PRE34380896) and the ARCS Foundation. The authors gratefully acknowledge support from DTRA (HDTRA1–15-1–0046) and NIH (R01NS106008 and R61 HL154252) to PCS, and MSCRF (MSCRFI-2784) and The NCI Physical Sciences-Oncology Center (U54CA210173) to SG.

## Nonstandard abbreviations

| | |
|---|---|
| **BBB** | Blood-brain barrier |
| **ECs** | Endothelial cells |
| **TJs** | Tight junctions |
| **hiPSC** | Human induced pluripotent stem cell |
| **iBMEC** | hiPSC-derived brain microvascular endothelial cell |

| | |
|---|---|
| **iPC** | hiPSC-derived pericyte |
| **PCM** | iPC-conditioned iBMEC media |
| **BM** | Basement membrane |
| **ECM** | Extracellular matrix |
| **FN** | Fibronectin |
| **TEER** | transendothelial electrical resistance |
| **iPSC** | Induced pluripotent stem cell |

## References


1. Abbott NJ, Patabendige AA, Dolman DE, Yusof SR, and Begley DJ (2010) Structure and function of the blood-brain barrier. Neurobiol Dis 37, 13–25 [PubMed: 19664713]
2. Daneman R, and Prat A (2015) The Blood–Brain Barrier. Cold Spring Harb Perspect Biol 7
3. Wong AD, Ye M, Levy AF, Rothstein JD, Bergles DE, and Searson PC (2013) The blood-brain barrier: an engineering perspective. Frontiers in neuroengineering 6, 7 [PubMed: 24009582]
4. Zhao Z, Nelson AR, Betsholtz C, and Zlokovic BV (2015) Establishment and Dysfunction of the Blood-Brain Barrier. Cell 163, 1064–1078 [PubMed: 26590417]
5. Prakash R, and Carmichael ST (2015) Blood-brain barrier breakdown and neovascularization processes after stroke and traumatic brain injury. Curr Opin Neurol 28, 556–564 [PubMed: 26402408]
6. Ogunshola OO, and Al-Ahmad A (2012) HIF-1 at the blood-brain barrier: a mediator of permeability? High Alt Med Biol 13, 153–161 [PubMed: 22994514]
7. Witt KA, Mark KS, Sandoval KE, and Davis TP (2008) Reoxygenation stress on blood-brain barrier paracellular permeability and edema in the rat. Microvasc Res 75, 91–96 [PubMed: 17651765]
8. Merali Z, Huang K, Mikulis D, Silver F, and Kassner A (2017) Evolution of blood-brain-barrier permeability after acute ischemic stroke. PLoS One 12, e0171558
9. Engelhardt S, Al-Ahmad AJ, Gassmann M, and Ogunshola OO (2014) Hypoxia selectively disrupts brain microvascular endothelial tight junction complexes through a hypoxia-inducible factor-1 (HIF-1) dependent mechanism. J Cell Physiol 229, 1096–1105 [PubMed: 24375098]
10. Page S, Raut S, and Al-Ahmad A (2019) Oxygen-Glucose Deprivation/Reoxygenation-Induced Barrier Disruption at the Human Blood-Brain Barrier is Partially Mediated Through the HIF-1 Pathway. Neuromolecular Med 21, 414–431 [PubMed: 30911877]
11. Engelhardt S, Patkar S, and Ogunshola OO (2014) Cell-specific blood-brain barrier regulation in health and disease: a focus on hypoxia. Br J Pharmacol 171, 1210–1230 [PubMed: 24641185]
12. Zieseniss A (2014) Hypoxia and the modulation of the actin cytoskeleton - emerging interrelations. Hypoxia (Auckl) 2, 11–21 [PubMed: 27774463]
13. Qi H, Wang P, Liu C, Li M, Wang S, Huang Y, and Wang F (2011) Involvement of HIF-1alpha in MLCK-dependent endothelial barrier dysfunction in hypoxia. Cell Physiol Biochem 27, 251–262 [PubMed: 21471714]
14. Wang P, Qi H, Sun C, He W, Chen G, Li L, and Wang F (2013) Overexpression of hypoxia-inducible factor-1alpha exacerbates endothelial barrier dysfunction induced by hypoxia. Cell Physiol Biochem 32, 859–870 [PubMed: 24081113]
15. Kuhlmann CR, Tamaki R, Gamerdinger M, Lessmann V, Behl C, Kempski OS, and Luhmann HJ (2007) Inhibition of the myosin light chain kinase prevents hypoxia-induced blood-brain barrier disruption. J Neurochem 102, 501–507 [PubMed: 17419808]
16. Chi AY, Waypa GB, Mungai PT, and Schumacker PT (2010) Prolonged hypoxia increases ROS signaling and RhoA activation in pulmonary artery smooth muscle and endothelial cells. Antioxid Redox Signal 12, 603–610 [PubMed: 19747063]

17. Kusuma S, Zhao S, and Gerecht S (2012) The extracellular matrix is a novel attribute of endothelial progenitors and of hypoxic mature endothelial cells. FASEB J 26, 4925–4936 [PubMed: 22919069]
18. Hayashi K, Nakao S, Nakaoke R, Nakagawa S, Kitagawa N, and Niwa M (2004) Effects of hypoxia on endothelial/pericytic co-culture model of the blood-brain barrier. Regul Pept 123, 77–83 [PubMed: 15518896]
19. Al Ahmad A, Gassmann M, and Ogunshola OO (2009) Maintaining blood-brain barrier integrity: pericytes perform better than astrocytes during prolonged oxygen deprivation. J Cell Physiol 218, 612–622 [PubMed: 19016245]
20. Kuntz M, Mysiorek C, Petrault O, Boucau MC, Aijjou R, Uzbekov R, and Berezowski V (2014) Transient oxygen-glucose deprivation sensitizes brain capillary endothelial cells to rtPA at 4h of reoxygenation. Microvasc Res 91, 44–57 [PubMed: 24333620]
21. Brillault J, Berezowski V, Cecchelli R, and Dehouck MP (2002) Intercommunications between brain capillary endothelial cells and glial cells increase the transcellular permeability of the blood-brain barrier during ischaemia. J Neurochem 83, 807–817 [PubMed: 12421352]
22. Lippmann ES, Azarin SM, Palecek SP, and Shusta EV (2020) Commentary on human pluripotent stem cell-based blood-brain barrier models. Fluids Barriers Cns 17, 64 [PubMed: 33076946]
23. Lippmann ES, Al-Ahmad A, Azarin SM, Palecek SP, and Shusta EV (2014) A retinoic acid-enhanced, multicellular human blood-brain barrier model derived from stem cell sources. Scientific Reports 4, 4160 [PubMed: 24561821]
24. Jamieson JJ, Linville RM, Ding YY, Gerecht S, and Searson PC (2019) Role of iPSC-derived pericytes on barrier function of iPSC-derived brain microvascular endothelial cells in 2D and 3D. Fluids Barriers Cns 16, 15 [PubMed: 31167667]
25. Citi S (2019) The mechanobiology of tight junctions. Biophys Rev 11, 783–793 [PubMed: 31586306]
26. Kusuma S, Shen Y-I, Hanjaya-Putra D, Mali P, Cheng L, and Gerecht S (2013) Self-organized vascular networks from human pluripotent stem cells in a synthetic matrix. PNAS 110, 12601–12606 [PubMed: 23858432]
27. Saunders JT, and Schwarzbauer JE (2019) Fibronectin matrix as a scaffold for procollagen proteinase binding and collagen processing. Mol Biol Cell 30, 2218–2226 [PubMed: 31242089]
28. Sabatier L, Chen D, Fagotto-Kaufmann C, Hubmacher D, McKee MD, Annis DS, Mosher DF, and Reinhardt DP (2009) Fibrillin assembly requires fibronectin. Mol Biol Cell 20, 846–858 [PubMed: 19037100]
29. Hielscher A, Ellis K, Qiu C, Porterfield J, and Gerecht S (2016) Fibronectin Deposition Participates in Extracellular Matrix Assembly and Vascular Morphogenesis. PLoS One 11, e0147600
30. Lu J, Doyle AD, Shinsato Y, Wang S, Bodendorfer MA, Zheng M, and Yamada KM (2020) Basement Membrane Regulates Fibronectin Organization Using Sliding Focal Adhesions Driven by a Contractile Winch. Dev Cell 52, 631–646 e634 [PubMed: 32004443]
31. Gudzenko T, and Franz CM (2015) Studying early stages of fibronectin fibrillogenesis in living cells by atomic force microscopy. Mol Biol Cell 26, 3190–3204 [PubMed: 26371081]
32. Davidson CD, Wang WY, Zaimi I, Jayco DKP, and Baker BM (2019) Cell force-mediated matrix reorganization underlies multicellular network assembly. Sci Rep 9, 12 [PubMed: 30626885]
33. Scott LE, Mair DB, Narang JD, Feleke K, and Lemmon CA (2015) Fibronectin fibrillogenesis facilitates mechano-dependent cell spreading, force generation, and nuclear size in human embryonic fibroblasts. Integr Biol (Camb) 7, 1454–1465 [PubMed: 26412391]
34. Humphrey JD, Dufresne ER, and Schwartz MA (2014) Mechanotransduction and extracellular matrix homeostasis. Nat Rev Mol Cell Biol 15, 802–812 [PubMed: 25355505]
35. Tornabene E, Helms HCC, Pedersen SF, and Brodin B (2019) Effects of oxygen-glucose deprivation (OGD) on barrier properties and mRNA transcript levels of selected marker proteins in brain endothelial cells/astrocyte co-cultures. PLoS One 14, e0221103
36. Baumann J, Huang SF, Gassmann M, Tsao CC, and Ogunshola OO (2019) Furin inhibition prevents hypoxic and TGFbeta-mediated blood-brain barrier disruption. Exp Cell Res 383, 111503

37. DeStefano JG, Jamieson JJ, Linville RM, and Searson PC (2018) Benchmarking in vitro tissue-engineered blood-brain barrier models. Fluids Barriers Cns 15
38. Underly RG, Levy M, Hartmann DA, Grant RI, Watson AN, and Shih AY (2017) Pericytes as Inducers of Rapid, Matrix Metalloproteinase-9-Dependent Capillary Damage during Ischemia. J Neurosci 37, 129–140 [PubMed: 28053036]
39. Stebbins MJ, Gastfriend BD, Canfield SG, Lee MS, Richards D, Faubion MG, Li WJ, Daneman R, Palecek SP, and Shusta EV (2019) Human pluripotent stem cell-derived brain pericyte-like cells induce blood-brain barrier properties. Sci Adv 5, eaau7375
40. Faal T, Phan DTT, Davtyan H, Scarfone VM, Varady E, Blurton-Jones M, Hughes CCW, and Inlay MA (2019) Induction of Mesoderm and Neural Crest-Derived Pericytes from Human Pluripotent Stem Cells to Study Blood-Brain Barrier Interactions. Stem Cell Rep 12, 451–460
41. Hicks K, O'Neil RG, Dubinsky WS, and Brown RC (2010) TRPC-mediated actin-myosin contraction is critical for BBB disruption following hypoxic stress. Am J Physiol Cell Physiol 298, C1583–1593 [PubMed: 20164382]
42. Engelhardt S, Huang SF, Patkar S, Gassmann M, and Ogunshola OO (2015) Differential responses of blood-brain barrier associated cells to hypoxia and ischemia: a comparative study. Fluids Barriers Cns 12, 4 [PubMed: 25879623]
43. Luissint AC, Artus C, Glacial F, Ganeshamoorthy K, and Couraud PO (2012) Tight junctions at the blood brain barrier: physiological architecture and disease-associated dysregulation. Fluids Barriers Cns 9
44. Nzou G, Wicks RT, VanOstrand NR, Mekky GA, Seale SA, El-Taibany A, Wicks EE, Nechtman CM, Marrotte EJ, Makani VS, Murphy SV, Seeds MC, Jackson JD, and Atala AJ (2020) Multicellular 3D Neurovascular Unit Model for Assessing Hypoxia and Neuroinflammation Induced Blood-Brain Barrier Dysfunction. Sci Rep 10, 9766 [PubMed: 32555384]
45. Rana MK, Srivastava J, Yang M, Chen CS, and Barber DL (2015) Hypoxia increases the abundance but not the assembly of extracellular fibronectin during epithelial cell transdifferentiation. J Cell Sci 128, 1083–1089 [PubMed: 25616899]
46. Hocking DC, Sottile J, and Langenbach KJ (2000) Stimulation of integrin-mediated cell contractility by fibronectin polymerization. J Biol Chem 275, 10673–10682 [PubMed: 10744764]
47. Lee TH, Hsieh ST, and Chiang HY (2019) Fibronectin inhibitor pUR4 attenuates tumor necrosis factor alpha-induced endothelial hyperpermeability by modulating beta1 integrin activation. J Biomed Sci 26, 37 [PubMed: 31096970]
48. Griggs LA, Hassan NT, Malik RS, Griffin BP, Martinez BA, Elmore LW, and Lemmon CA (2017) Fibronectin fibrils regulate TGF-beta1-induced Epithelial-Mesenchymal Transition. Matrix Biol 60–61, 157–175
49. Varadaraj A, Jenkins LM, Singh P, Chanda A, Snider J, Lee NY, Amsalem-Zafran AR, Ehrlich M, Henis YI, and Mythreye K (2017) TGF-beta triggers rapid fibrillogenesis via a novel TbetaRII-dependent fibronectin-trafficking mechanism. Mol Biol Cell 28, 1195–1207 [PubMed: 28298487]
50. Yamashita M, Aoki H, Hashita T, Iwao T, and Matsunaga T (2020) Inhibition of transforming growth factor beta signaling pathway promotes differentiation of human induced pluripotent stem cell-derived brain microvascular endothelial-like cells. Fluids Barriers Cns 17, 36 [PubMed: 32456699]

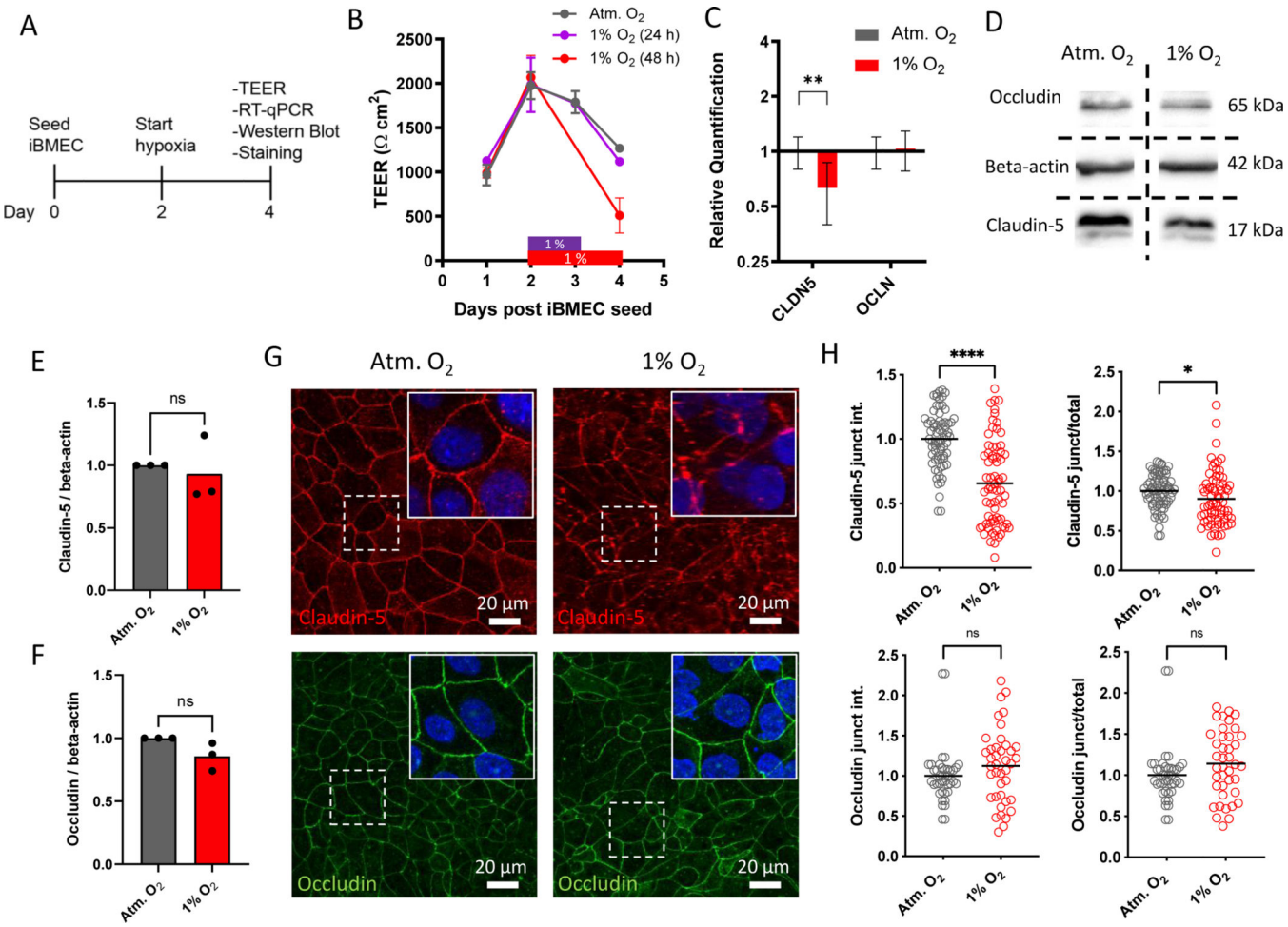


**Figure 1. Hypoxia decreases barrier function by disrupting junctional claudin-5.**

(A) Experimental timeline. (B) Time dependence of TEER values for iBMEC monolayers exposed to hypoxia for 24 or 48 h. Data represent mean ± SD of duplicate Transwells in a representative differentiation. (C) RT-qPCR for claudin-5 and occludin after 48 h exposure to atmospheric $O_2$ or 1% $O_2$. Data represent mean ± SD, n = 3 independent differentiations. (D) Representative western blot for claudin-5, occludin, and beta-actin after 48 h exposure to atmospheric $O_2$ or 1% $O_2$. (E-F) Quantifications of WB for claudin-5 and occluding, each normalized to beta-actin loading control, n = 3 independent differentiations. Both bands appearing for claudin-5 in (D) were included in this quantification. (G) Representative max intensity projections of confocal immunofluorescence images of claudin-5 and occludin after 48 h exposure to atmospheric $O_2$ or 1% $O_2$. Insets also show cell nuclei labeled with DAPI. (H) Junctional and junctional/total intensities of claudin-5 (top) and occludin (bottom). Junctional and junctional/total intensities represent n = 70 cells from three independent differentiations (claudin-5) and n = 40 cells from two independent differentiations (occludin). Statistical significance levels are set at * $p < 0.05$, ** $p < 0.01$, *** $p < 0.001$, and **** $p < 0.001$.

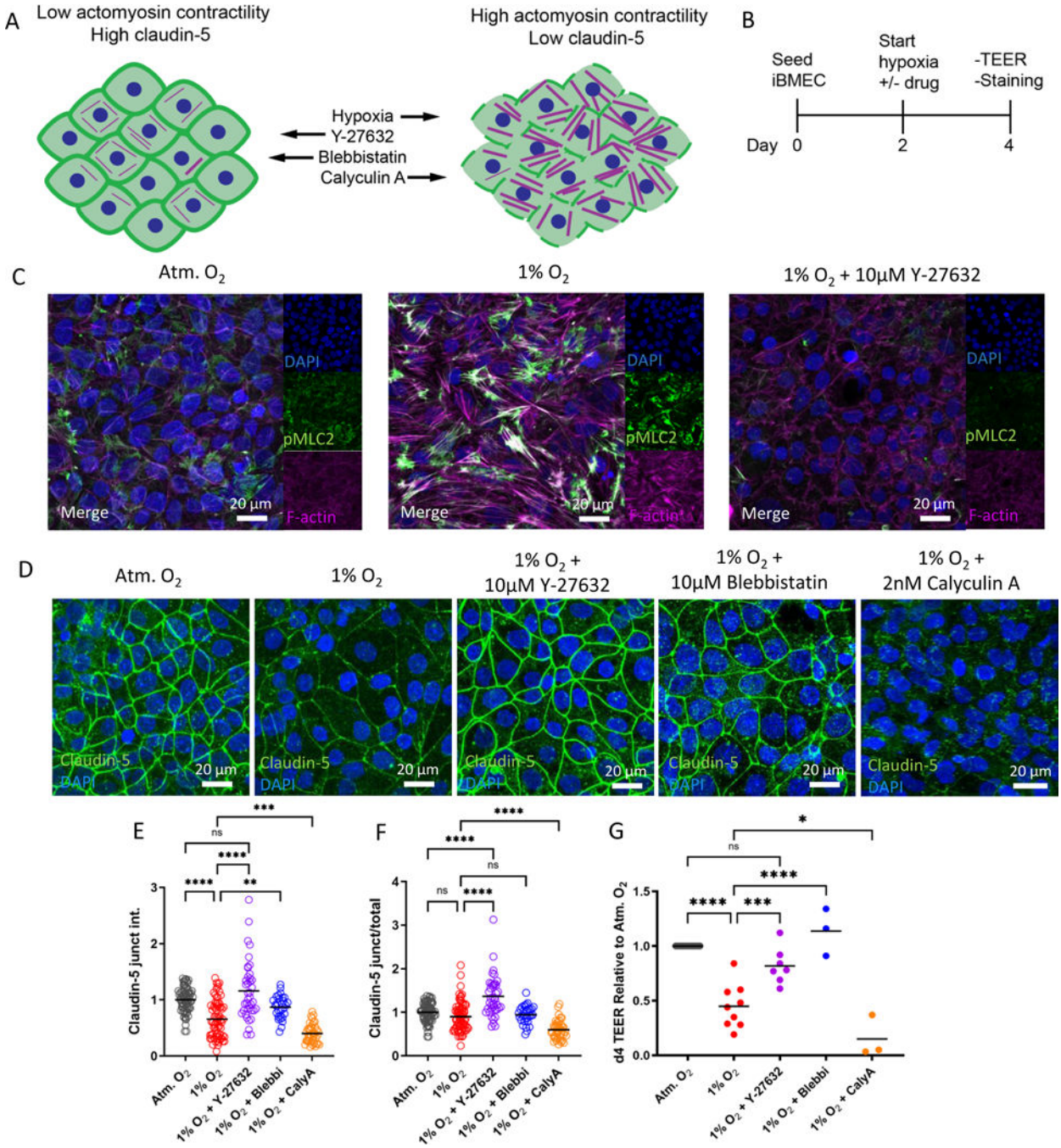


**Figure 2. Hypoxia modulates claudin-5 via increased actomyosin contractility.**

(A) Schematic illustration of proposed relationship between hypoxia, actomyosin contractility, and claudin-5. (B) Experimental timeline. (C) Representative max intensity projections of confocal immunofluorescence images of pMLC2 and F-actin after 48 h exposure to atmospheric $O_2$, 1% $O_2$, or 1% $O_2$ with Y-27632. (D) Representative max intensity projections of confocal immunofluorescence images of claudin-5 after 48 h exposure to atmospheric $O_2$, 1% $O_2$, 1% $O_2$ with addition of Y-27632 or blebbistatin to reduce contractility, or 1% $O_2$ with calyculin-A to increase contractility. (E-F) Junctional

and junctional/total intensities of claudin-5. Junctional and junctional/total intensities represent n = 30 – 70 cells from 3 – 4 independent differentiations. (G) TEER for iBMEC monolayers after 48 h exposure to atmospheric $O_2$, 1% $O_2$, or 1% $O_2$ with addition of Y-27632, blebbistatin, or calyculin-A. TEER is expressed relative to iBMEC maintained in atmospheric $O_2$. Data represent n = 3 – 10 Transwells per condition pooled from 3 – 5 independent iBMEC differentiations. Statistical significance levels are set at * $p < 0.05$, ** $p < 0.01$, *** $p < 0.001$, and **** $p < 0.001$.

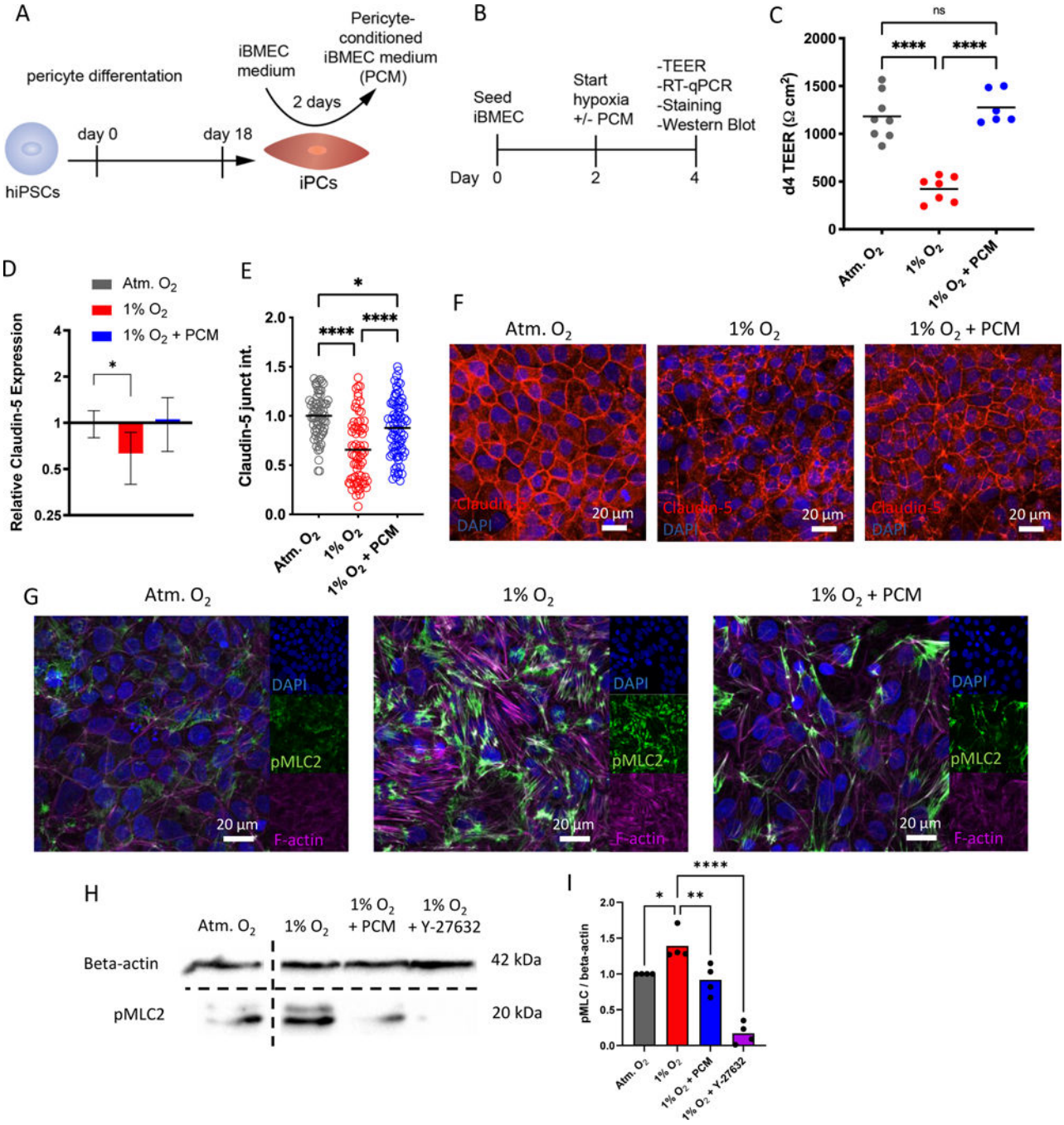


**Figure 3. Pericyte-conditioned media improves endothelial barrier during hypoxia via normalized cell contractility and claudin-5 stabilization.**

(A) Schematic illustration of iPC differentiation and collection of iPC-conditioned iBMEC medium (PCM). (B) Experimental timeline. (C) TEER values after 48 h exposure to atmospheric $O_2$, 1% $O_2$, or 1% $O_2$ in PCM. Data represent n = 6 – 8 Transwells per condition pooled from 3 – 4 independent iBMEC differentiations. (D) RT-qPCR for claudin-5 and occludin after 48 h exposure to atmospheric $O_2$, 1% $O_2$, or 1% $O_2$ in PCM. Data represent mean ± SD from 3 independent differentiations. (E) Junctional intensity of claudin-5. Data represent n = 70 – 80 cells per condition pooled from

4 independent iBMEC differentiations. (F) Representative max intensity projections of confocal immunofluorescence images of claudin-5 after 48 h exposure to atmospheric $O_2$, 1% $O_2$, or 1% $O_2$ in PCM. (G) Representative maximum intensity projections of confocal immunofluorescence images of pMLC2 and F-actin after 48 h exposure to atmospheric $O_2$, 1% $O_2$, or 1% $O_2$ in PCM. (H) Representative western blot for pMLC2 and beta-actin after 48 h exposure to atmospheric $O_2$, 1% $O_2$, 1% $O_2$ in PCM, or 1% $O_2$ with Y-27632. (I) Quantification of WB for pMLC2 normalized to beta-actin loading control. Both bands appearing for pMLC2 in (H) were included in this quantification. Bars represent mean values. Individual points correspond to 4 independent iBMEC differentiations. Statistical significance levels are set at * $p < 0.05$, ** $p < 0.01$, *** $p < 0.001$, and **** $p < 0.001$.

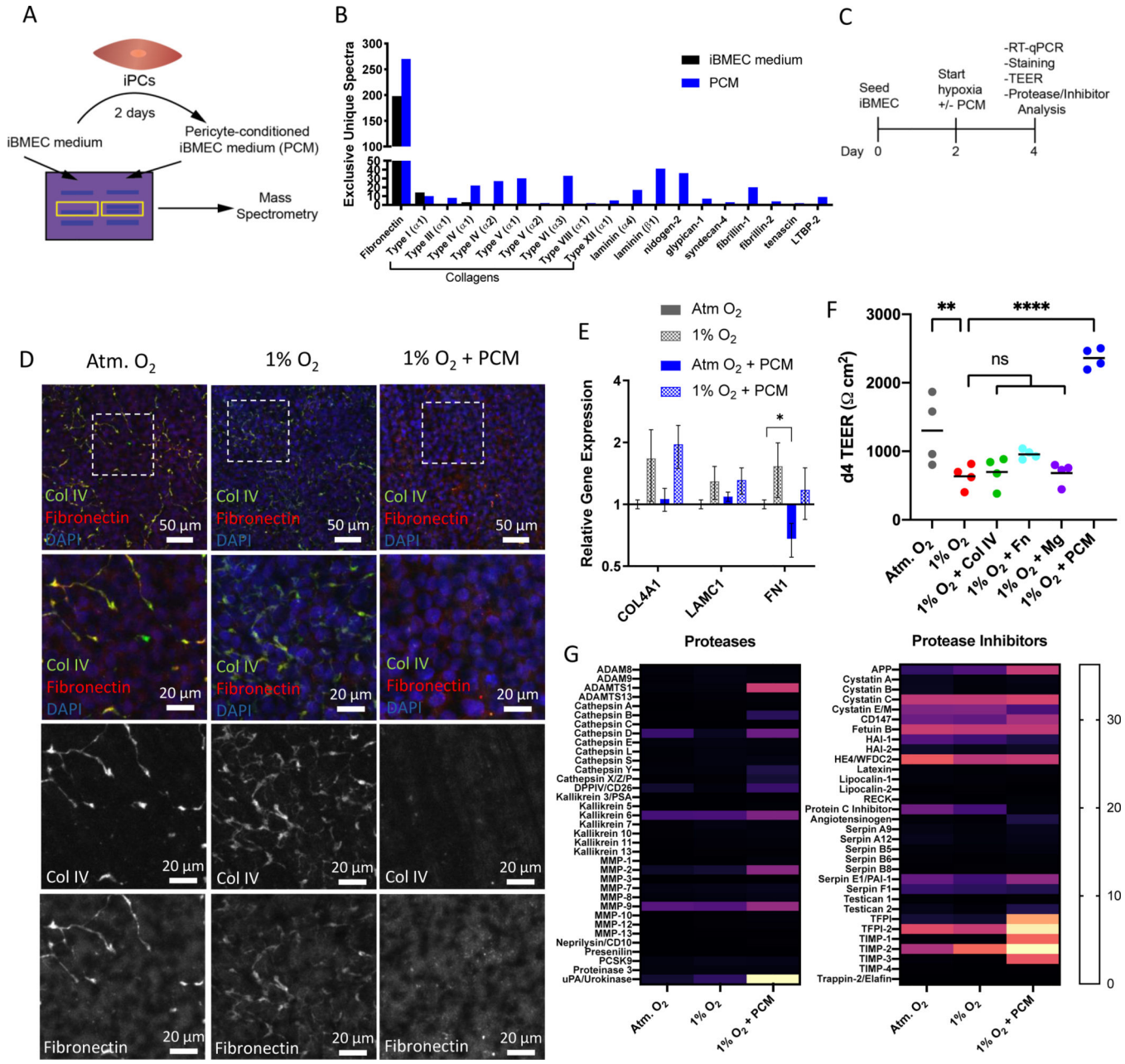


**Figure 4. Hypoxia and PCM alter basement membrane organization in iBMEC monolayers.**

(A) Schematic illustration of analysis of standard iBMEC medium and PCM via SDS-PAGE and mass spectrometry proteomics. (B) Mass spectrometry analysis of excised SDS-PAGE gel regions from standard iBMEC medium and PCM. n = 3 lot-matched pairs of iBMEC and PCM were used for SDS-PAGE and one was analyzed via mass spectrometry proteomics. Select ECM or ECM-related proteins are displayed. Complete results are listed in Table S1. (C) Experimental timeline. (D) Representative max intensity projections of confocal immunofluorescence images of collagen IV and fibronectin in iBMEC monolayers on Transwells after 48 h exposure to atmospheric $O_2$, 1% $O_2$, or 1% $O_2$ in PCM. (E) RT-qPCR for collagen IV (COL4A1), laminin (LAMC1), and fibronectin (FN1) after 48 h exposure to

atmospheric $O_2$, 1% $O_2$, atmospheric $O_2$ in PCM, or 1% $O_2$ in PCM. Data represent mean ± SD from 3 independent differentiations. (F) TEER after 48 h exposure to atmospheric $O_2$, 1% $O_2$, 1% $O_2$ with the addition of soluble collagen IV (Col IV), fibronectin (Fn), or Matrigel (Mg), or 1% $O_2$ in PCM. Data represent n = 4 Transwells pooled from two independent iBMEC differentiations. (G) Antibody arrays for proteases and protease inhibitors detected in media from iBMECs after 48 h exposure to atmospheric $O_2$, 1% $O_2$, or 1% $O_2$ in PCM. Heat maps are displayed in arbitrary units and represent mean values of n = 2 arrays performed on independent iBMEC differentiations. Statistical significance levels are set at * $p < 0.05$, ** $p < 0.01$, *** $p < 0.001$, and **** $p < 0.001$.

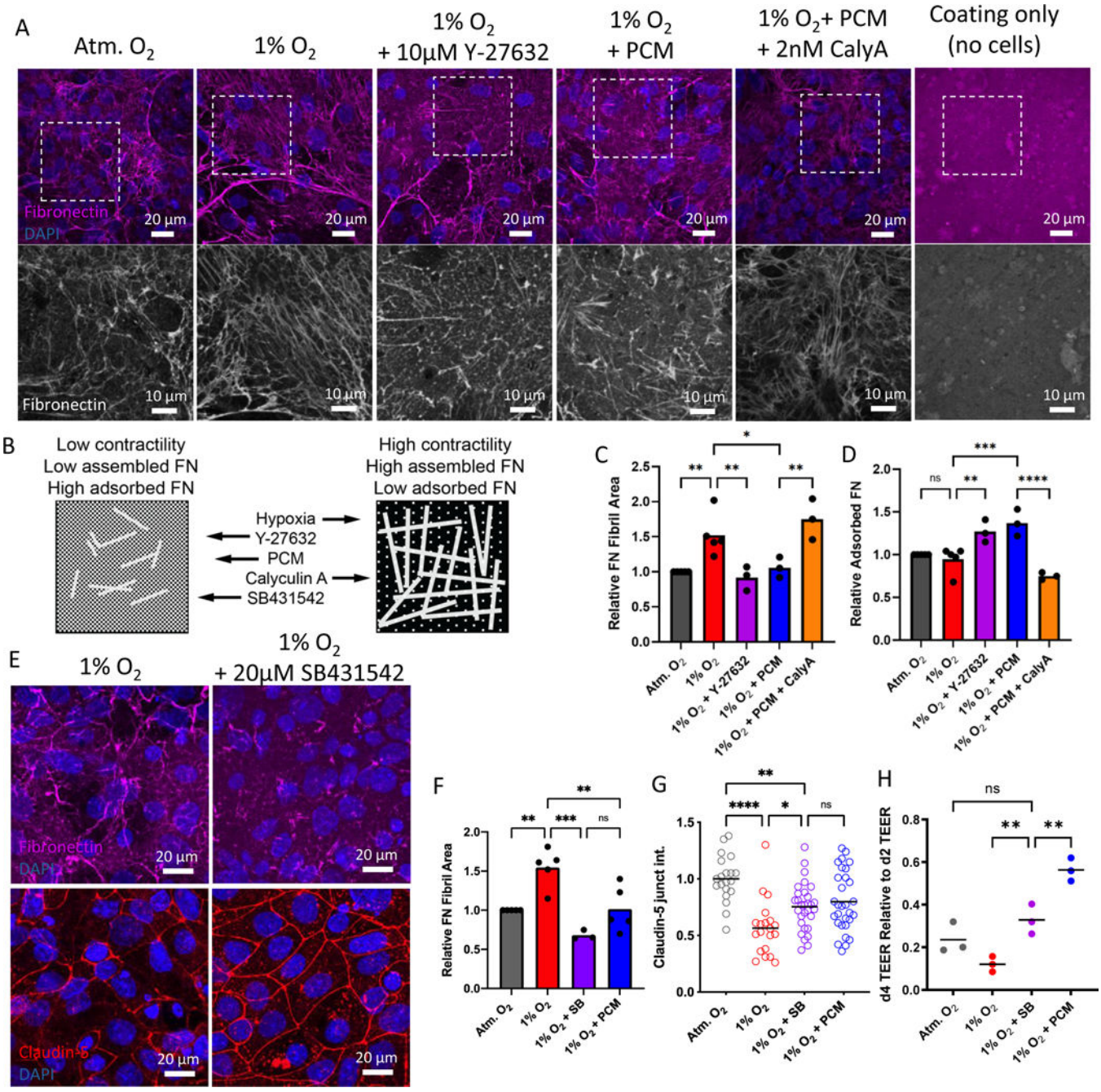


**Figure 5. Fibronectin fibrillogenesis is dependent upon cellular contractility and is accelerated in hypoxia but attenuated by PCM or TGF-β inhibition.**

(A) Representative max intensity projections of confocal immunofluorescence images of fibronectin after 48 h exposure to atmospheric $O_2$, 1% $O_2$, 1% $O_2$ with addition of Y-27632 to reduce contractility, 1% $O_2$ in PCM, and 1% $O_2$ in PCM with the addition of calyculin-A to increase contractility. The 'coating only' condition demonstrates the appearance of adsorbed Fn from the Col IV/Fn coating. (B) Graphic depiction of the proposed relationship between contractility and fibronectin fibrillogenesis. (C) Fibronectin fibril area, quantified for the conditions shown in (A). n = 3 – 5 images per condition pooled from two

independent differentiations. (D) Adsorbed fibronectin, quantified for the conditions shown in (A). n = 3 – 5 images per condition pooled from two independent differentiations. (E) Representative max intensity projections of confocal immunofluorescence images of fibronectin (top) and claudin-5 (bottom) after 48 h exposure to 1% $O_2$ with or without SB431542 to inhibit TGF-β signaling. (F) Fibronectin fibril area after 48 h exposure to 1% $O_2$, 1% $O_2$ with SB431542, or 1% $O_2$ in PCM. n = 3 – 5 images per condition pooled from two independent differentiations. (G) Junctional intensity of claudin-5. Data represent n = 20 – 30 cells per condition pooled from two independent differentiations. (H) TEER after 48 h exposure to 1% $O_2$, 1% $O_2$ with SB431542, or 1% $O_2$ in PCM. Bars represent mean values. Individual points correspond with n = 3 Transwells pooled from two independent iBMEC differentiations. Statistical significance levels are set at * $p < 0.05$, ** $p < 0.01$, *** $p < 0.001$, and **** $p < 0.001$.